

Article

Development of Binder Free Interconnected 3D Flower of NiZn₂O₄ as an Advanced Electrode Materials for Supercapacitor Applications

Sajid Ali Ansari ^{1,*} , Nazish Parveen ², Mohd Al Saleh Al-Othoum ¹ and Mohammad Omaish Ansari ³ 

¹ Department of Physics, College of Science, King Faisal University, P.O. Box 400, Hofuf, Al-Ahsa 31982, Saudi Arabia; malothoum@kfu.edu.sa

² Department of Chemistry, College of Science, King Faisal University, P.O. Box 380, Hofuf, Al-Ahsa 31982, Saudi Arabia; nislam@kfu.edu.sa

³ Center of Nanotechnology, King Abdulaziz University, Jeddah 21589, Saudi Arabia; moansari@kau.edu.sa

* Correspondence: sansari@kfu.edu.sa; Tel.: +966-13-589-9598

Abstract: The design and development of electrode materials for energy-storage applications is an area of prime focus around the globe because of the shortage of natural resources. In this study, we developed a method for preparing a novel three-dimensional binder-free pseudocapacitive NiZn₂O₄ active material, which was grown directly over nickel foam (NiZn₂O₄@3D-NF), using a simple one-step hydrothermal process. The material was characterized by X-ray diffraction, scanning electron microscopy, and transmission electron microscopy. Cyclic voltammetry, galvanostatic charge-discharge, and electrochemical impedance spectroscopy techniques were employed to evaluate the pseudocapacitive performance of the NiZn₂O₄ active material in a three-electrode assembly cell. The prepared NiZn₂O₄@3D-NF electrode exhibited an excellent specific capacitance, of 1706.25 F g⁻¹, compared to that of the NiO@3D-NF (1050 F/g) electrode because it has the bimetallic characteristics of both zinc and nickel. The NiZn₂O₄@3D-NF electrode showed better cyclic stability (87.5% retention) compared to the NiO@3D-NF electrode (80% retention) after 5000 cycles at a fixed current density, which also supports the durability of the NiZn₂O₄@3D-NF electrode. The characteristics of NiZn₂O₄@3D-NF include corrosion resistance, high conductivity, an abundance of active sites for electrochemical reaction, a high surface area, and synergism between the bimetallic oxides, which make it a suitable candidate for potential application in the field of energy storage.

Keywords: energy storage; bimetallic oxides; supercapacitor; electrodes; three-dimensional



Citation: Ansari, S.A.; Parveen, N.; Al-Othoum, M.A.S.; Ansari, M.O. Development of Binder Free Interconnected 3D Flower of NiZn₂O₄ as an Advanced Electrode Materials for Supercapacitor Applications. *Crystals* **2022**, *12*, 14. <https://doi.org/10.3390/cryst12010014>

Academic Editor: Faxing Wang

Received: 4 December 2021

Accepted: 18 December 2021

Published: 22 December 2021

Publisher's Note: MDPI stays neutral with regard to jurisdictional claims in published maps and institutional affiliations.



Copyright: © 2021 by the authors. Licensee MDPI, Basel, Switzerland. This article is an open access article distributed under the terms and conditions of the Creative Commons Attribution (CC BY) license (<https://creativecommons.org/licenses/by/4.0/>).

1. Introduction

With the increasing demand for portable devices, whose function is supported by energy-storage electrodes, much attention in research has focused on energy storage in the development of sustainable alternatives that allows for reducing fossil fuel consumption [1–3]. For this purpose, efforts have also been focused on developing various innovations for new energy-storage materials and devices, such as batteries and supercapacitors, for numerous important reasons [2–7]. Supercapacitors (SCs) have advantages compared to batteries, such as low internal resistance, long life, power density, light weight, and portability. SCs can be categorized according to the mechanism of electrochemical reaction during the charge–discharge process [8–10]. The rapid faradaic redox reaction that occurs during the electrochemical reaction is characteristic of SCs of the pseudocapacitor category, and the interface between the electrolyte and the electrode surface during the electrochemical process characterizes SCs of the double-layered capacitor category. These categories can also be further divided according to the use of identical or different electrode-assembled SCs (symmetric or asymmetric SCs) [11–13].

The lifecycle of SCs is totally dependent on the active materials used to prepare the electrode, which are the key components of the assembly cell. For this purpose, various types of active materials, such as carbon-based materials, oxide, sulfides, hydroxide, bimetallic

three-dimensional materials, and conducting polymers, have been used to develop efficient electrodes for supercapacitor cells [14–17]. Among them, binary transition metal-based electrode materials have gained attention in various applications, including in energy-storage devices, because of their unique structures and properties, such as the synergistic effect created by the presence of the two metals. Better electrochemical performance, a high specific capacitance, and long cyclic stability are the main features that make these materials potential candidates in the field of energy-storage application. In addition, the spinel structure of metal oxides in bimetallic oxides remains the same because the metal easily replaces the atoms from the material counterparts, which can also be helpful to enhance the faradaic redox reaction site, which, in turn, helps to increase the specific capacitance of bimetallic oxide-based electrodes. Therefore, the selection of the appropriate bimetallic oxide and its rational structure are important for enhancing the overall performance and for ensuring structural stability during the electrochemical charge–discharge process [14–20].

In addition, metal oxides and sulfide-based electrodes have been used as positive electrodes in various pseudocapacitors because of their good electrical conductivity, their lower electronegativity, and their redox behavior. The metal sulfides, such as NiS, NiS₂, and MoS₂, have received much attention in fabricated energy-storage electrode materials [21]. Apart from the aforementioned advantages, there are some problems associated with metal sulfides, firstly, due to the insulating nature of sulfur, which may be responsible for the poor stability of the electrodes. Secondly, the fluctuations and the expansion of the sulfides are thermodynamically unstable. Third, oxidation and the volatile nature of the metal sulfides, due to acidity, are common problems for their practical application [22]. The metal oxides, such as Co₂O₄, MnO₂, and NiO, are proposed as efficient electrode materials for supercapacitor applications. Among these are nickel-based materials, which have morphological diversities that include rods, wires, flowers, etc. The NiO can offer excellent electrochemical performance and good electrical conductivity with binder-free-based material compared to other metal oxides. However, the performance with the NiO-based materials has the limitations of low specific capacitance, slow rate stability, poor durability, and low redox activities in the charge–discharge process [8,23]. To overcome these situations, many researchers have fabricated electrodes based on mixed/binary metal oxides, such as Xu et al. [24], who prepared NiCr₂O₄ chromite spinel via the precipitation method using aqueous ammonium solution, which exhibited a specific capacitance of 187 F/g at a current density of 0.6 A/g. Xu et al. [25] fabricated a nanobelt of ZnCo₂O₄ via the hydrothermal method using hexamethylenetetramine, which acts as an adsorptive alkali, and it showed a specific capacitance of 229 F/g. Sahoo et al. [26] used the electrodeposition technique to develop MnCo₂O₄ nanosheets over glass substrates coated in indium-doped tin oxide (ITO), with a specific capacitance of 250 F/g. Xu et al. [27] fabricated NiCo₂O₄ active materials using the hydrothermal method, and improved the specific capacitance up to 273.5 F/g with the help of activated carbon. Similarly, Kumar et al. [8] prepared flower-like NiZn₂O₄ over a nickel foam substrate, which showed a 253 F/g specific capacitance at a 1 A/g current density. These binary metal oxide electrodes delivered improved electrochemical energy-storage performances compared to the simple and individual metal oxides [28,29]. Even though NiO₂ and ZnO₂ electrode materials have shown high-energy-storage performances, the literature on mixed Ni–Zn electrode materials is very limited. Thus, the synthesis of NiZn₂O₄ as an effective electrode material would be beneficial because of the merits of the low cost, the binder-free nontoxicity, and the superior electrochemical specific capacitance from the synergistic effect of the Ni and Zn ions.

However, other bimetallic oxides, especially NiZn₂O₄, have rarely been used as active materials for electrochemical supercapacitive applications, although they have characteristics similar to other metal-based bimetallic electrode materials, and individual oxides of nickel and zinc have been investigated for energy-storage applications. Therefore, it is worth studying the electrochemical performance of a mixed nickel–zinc binary oxide for the supercapacitive performance in order to determine its suitability as a potential candidate for energy-storage applications on the basis of the possession of various ad-

vantages, such as low costs, being binder-free, excellent specific capacitance, and superior electrochemical properties owing to the synergistic effects. Therefore, in this study, we used a single-step hydrothermal process to prepare a three-dimensional binder-free flower-like bimetallic NiZn₂O₄ active material (NiZn₂O₄@3D-NF), and we investigated the electrochemical supercapacitive performance in detail using the cyclic voltammetry, galvanostatic charge–discharge, and electrochemical impedance spectroscopy techniques. The NiZn₂O₄@3D-NF delivered a high specific capacitance of 1706.25 F/g, compared to the NiO@3D-NF (1050 F g^{−1}) at the same current density of 1.5 A/g, in addition to delivering excellent cyclic stability over 5000 cycles (87.5% retention).

2. Experimental

2.1. Materials

Zinc sulfate, nickel(II) sulfate, hexamethylenetetramine, N-methyl-2-pyrrolidone, potassium hydroxide, ethyl alcohol, and acetone were acquired from Sigma-Aldrich. Nickel foam (>99.99% purity) was obtained from the MTI Corporation, U.S.A. Polyvinylidene fluoride was procured from the Daejung Chemicals and Metal Co., Ltd., Korea.

2.2. Methods

A PANalytical X-ray diffractometer (X'pert PRO-MPD, The Netherlands), with $\lambda = 0.15405$ nm, was used to investigate the phases and the crystal structure of the NiZn₂O₄@Ni foam. Field emission transmission electron microscopy (FE-TEM), at an accelerating voltage of 200 kV (Tecnai G2 F20, FEI, College Station, TX, USA), was used to evaluate the morphology and surface behavior of the NiZn₂O₄@3D-NF.

2.3. Electrochemical Measurements

The electrochemical pseudocapacitive performance of the NiZn₂O₄ active material was evaluated by galvanostatic charge–discharge (GCD), cyclic voltammetry (CV), and electrochemical impedance spectroscopy techniques, inside three assembly cells. During all of the electrochemical supercapacitor measurements, the active area was fixed to 1 cm × 1 cm of the fabricated binder-free NiO@3D-NF and the NiZn₂O₄@3D-NF. A VersaSTAT 3 potentiostat workstation (Princeton Research, Princeton, NJ, USA), connected with working, reference (Ag/AgCl), and counter (Pt plate) electrodes, was used to evaluate the electrochemical performance. Aqueous potassium hydroxide was used as the active electrolyte for the electrochemical measurements [14].

$$C = \frac{I dt}{m dV} \quad (1)$$

where C represents the specific capacitance (F/g); t represents the discharging time; m is the mass of the active materials coated/grown over the current collector; dV represents the applied potential window; and I represents the applied current and is the applied potential window.

$$E = 1/2 CV^2 \quad (2)$$

$$P = E/t \quad (3)$$

where E is the energy density; C is the specific capacitance of the NiZn₂O₄@3D-NF-fabricated electrode; V denotes the applied voltage window; and t represents the discharge times.

2.4. Synthesis of Binder-Free Bimetallic NiZn₂O₄@3D-NF Active Material

The three-dimensional flower-like NiZn₂O₄ was grown over nickel foam (NiZn₂O₄@3D-NF) via a simple and cost-effective hydrothermal process, using zinc sulfate (ZnSO₄·7H₂O), nickel sulfate (NiSO₄·6H₂O), and hexamethylenetetramine (C₆H₁₂N₄) as the starting precursors. For this process, initially, a piece of nickel foam (Figure S1, in Supplementary Materials) with a size of 1 × 3 cm, was washed with 1-M hydrochloric acid solution, ethanol,

and DI water, followed by ultrasonication to remove the oxidized layer present over the surface. Next, 0.2875 g of $\text{ZnSO}_4 \cdot 7\text{H}_2\text{O}$, and 0.2321 g of $\text{NiSO}_4 \cdot 6\text{H}_2\text{O}$, were dissolved in 50 mL of a $\text{C}_6\text{H}_{12}\text{N}_4$ aqueous solution, and were further stirred for 15 min at 60 °C. The resulting mixture was transferred to a Teflon-lined stainless autoclave, in which the nickel foam (1 cm × 3 cm) substrate was dipped. After that, the autoclave was carefully sealed and placed in an electric oven at 150 °C for 5 h. After completion of the reaction, the resulting precipitate was washed with water and ethanol, dried at 80 °C for 12 h, and was then stored in a desiccator for further study. The three-dimensional flower-like NiZn_2O_4 grown over the nickel foam is abbreviated as $\text{NiZn}_2\text{O}_4@3\text{D-NF}$ (Figure 1). For the comparative study, nickel oxide was also grown over nickel foam under similar experimental conditions, and it is abbreviated as $\text{NiO}@3\text{D-NF}$.

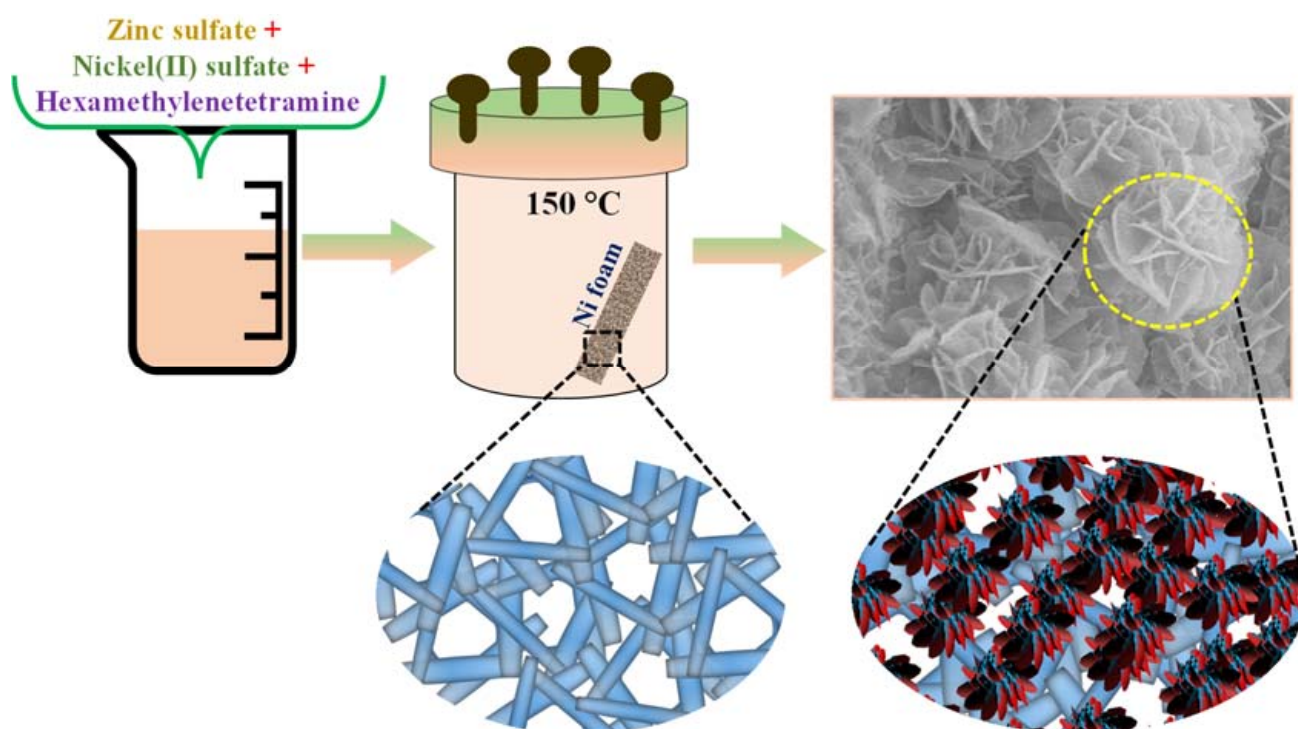


Figure 1. Schematic illustration of the synthesis of binder-free $\text{NiZn}_2\text{O}_4@3\text{D-NF}$.

3. Results and Discussion

3.1. XRD and FESEM Analysis

The crystal structure and the phases of the $\text{NiZn}_2\text{O}_4@3\text{D-NF}$ were examined by XRD, and the results are depicted in Figure 2a, which shows the mixed pattern of nickel- and zinc-based bimetallic oxides. The peaks observed at 36.90° , 43.15° , and 61.00° 2θ , corresponding to the planes of (111), (200), and (220), respectively, show good correspondence with the cubic phase of nickel oxide (JCPDS No. 47-1049) [8]. The diffraction patterns observed at 34.50° , 36.50° , and 61.94° 2θ can be readily indexed to the standard planes of (002), (101), and (103), respectively, corresponding to the hexagonal phase of NiZn_2O_4 (JCPDS No. 36-14541). The few diffraction peaks are merged, which also supports the successful formation of NiZn_2O_4 . A few broad diffraction peaks of low intensity indicate the low crystalline nature of NiZn_2O_4 . However, the left shifting of the peak in the NiZn_2O_4 clearly signifies the doping of the zinc ion to the nickel sites, which also suggests the crystalline behavior of NiZn_2O_4 . It is well known that the use of an appropriate preparation process will result in the retention of a crystal structure, which can manifest as rigidity during expansion while undergoing intense electrochemical measurements.

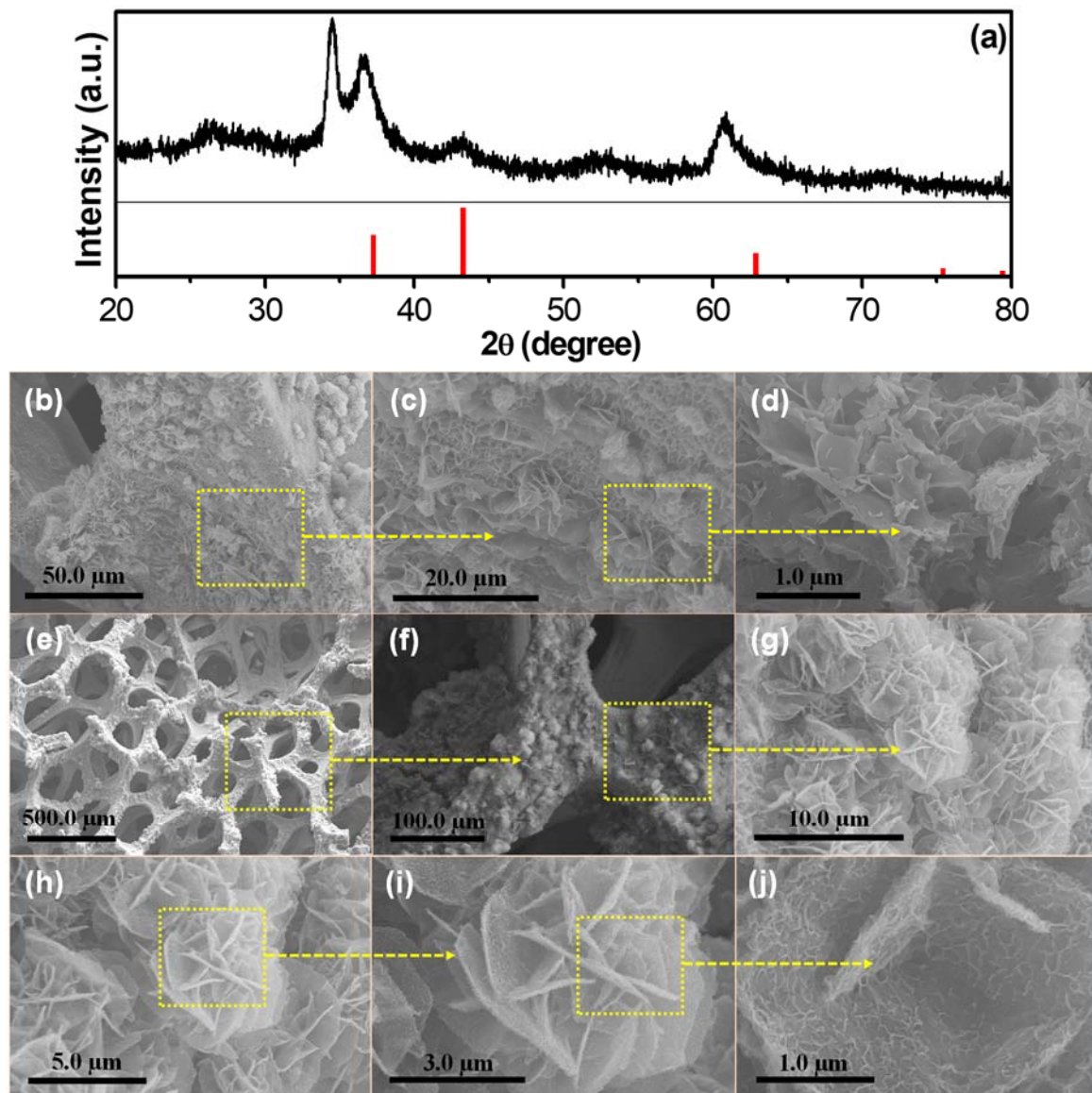


Figure 2. (a) XRD patterns of NiZn₂O₄@3D-NF, and FE-SEM images of (a–c) nickel oxide, and (d–j) NiZn₂O₄@3D-NF at different magnifications.

The morphologies and microstructures of the 3D-nanosheet-assembled porous flower-like pure NiO@3D-NF and the NiZn₂O₄@3D-NF electrode material were investigated by FESEM analysis. Figure 2b–d shows SEM images of NiO@3D-NF at a lower magnification than the FESEM images. Figure 2d shows the abundant thin nanosheet-like morphology of homogeneous growth on the conductive current collector (Ni foam) that forms a 3D flower-like morphology. Observation at higher magnification clearly illustrates that these thin sheets all exhibit an irregular shape and size. With regard to the binary composite (NiZn₂O₄@3D-NF), it can be clearly seen at lower magnification (Figure 2e–j) that numerous sheet-like structures grew homogeneously on the Ni foam and assembled into a 3D flower-like structure. The size of the 3D flower morphology of the binary composite is 5–7 μm, the diameter of the nanosheet is about 2–4 μm, and the thickness of the nanosheet is 40–50 nm, as measured from the high-magnification FESEM images in Figure 2i,j. Moreover, using high magnification, it can also be clearly seen in the FESEM images that several burr-like structures grew on the surface of the nanosheet. These burr-like structures provide a larger contact area between the synthesized electrode material and the electrolyte compared to

the pure nanosheet, which helps to enhance the electrochemical properties of the electrode material for its favorable application in various energy-storage applications.

3.2. TEM and HRTEM Analysis

TEM and HRTEM were further employed to examine the internal structures and surface morphologies of the NiO@3D-NF and the NiZn₂O₄@3D-NF, and the results are shown in Figure 3. Figure 3a,b shows TEM images of NiO, which reveal the rather large flower size, as well as a structure that is not very porous. However, the TEM and HRTEM images of the bimetallic NiZn₂O₄@3D-NF (Figure 3c–f) clearly show the morphology and porous behavior, which are in accordance with the FESEM analysis. Figure 3c,d clearly show that the NiZn₂O₄@3D-NF consists of numerous interconnected petal-like structures. This unique morphology, with an interconnected structure, certainly plays an important role in the electrochemical reaction that occurs between the electrode and the electrolytes. In addition, the presence of the radial sphere reduces the path length of ion diffusion during electrochemical measurements. These results are also in accordance with the abovementioned SEM analysis.

3.3. Electrochemical Studies

The three-electrode assembly cell was connected with the potentiostat/galvanostat workstation setup to evaluate the electrochemical performance using the CV (Figures S2a and 4a,c,d), GCD (Figures S2b and 4b,e,f), and EIS (Figure 5b) techniques, which are proficient tools for examining the capacitive behavior of active materials. Figure 4a shows a comparative CV graph of the NiO@3D-NF and the NiZn₂O₄@3D-NF, recorded within the potential window range of 0.0–0.5 V, and at a fixed scan rate of 30 mV s^{−1}. The CV graph of NiO@3D-NF and NiZn₂O₄@3D-NF shows clear redox peaks at ~0.31 and 0.37 V within the defined potential window, clearly indicating the pseudocapacitive behavior of the fabricated electrode. The redox reaction involving the potassium hydroxide electrolyte included two steps, which corresponded, respectively, to the reversible reaction of the M²⁺/M³⁺ transitions (M = Ni, Co, Zn, Cu, etc.) associated with the OH[−] ions. Even at a high scan rate, the CV curves depict well-defined redox peaks, which clearly indicates that the fabricated binder-free NiZn₂O₄@3D-NF electrode fully sustained the rapid redox reaction. The CV curves also suggest that, at a high scan rate, the peak slightly shifted to the initial position, which indicates the lower polarization of the electrode materials, and the fast electron and ion transport rates during electrochemical processes. On the basis of an electroanalytical point of view, the small potential difference in the anodic and cathodic peaks may be attributed to the reversible electrochemical reaction, which can be explained with the help of the following reaction, Equations (4) and (5) [8,9]:



The comparative CV profile shows that the integrated capacitive area is larger for NiZn₂O₄@3D-NF than for NiO@3D-NF, which is also the basis for the better electrochemical supercapacitive performance of the NiZn₂O₄@3D-NF. The improved electrochemical performance of NiZn₂O₄@3D-NF compared to NiO@3D-NF is due to the large area provided to the electrolyte ions, which can be easily penetrated during the electrochemical process. The CV graph of the NiO@3D-NF and the NiZn₂O₄@3D-NF was recorded at different scan rates, and the results are shown in Figure 4c,d. The results show that the reversibility and integrated capacitive area of the electrode during the faradaic reaction was homogeneously maintained, even at higher scan rates, which supports increased ion diffusion during the electrochemical process.

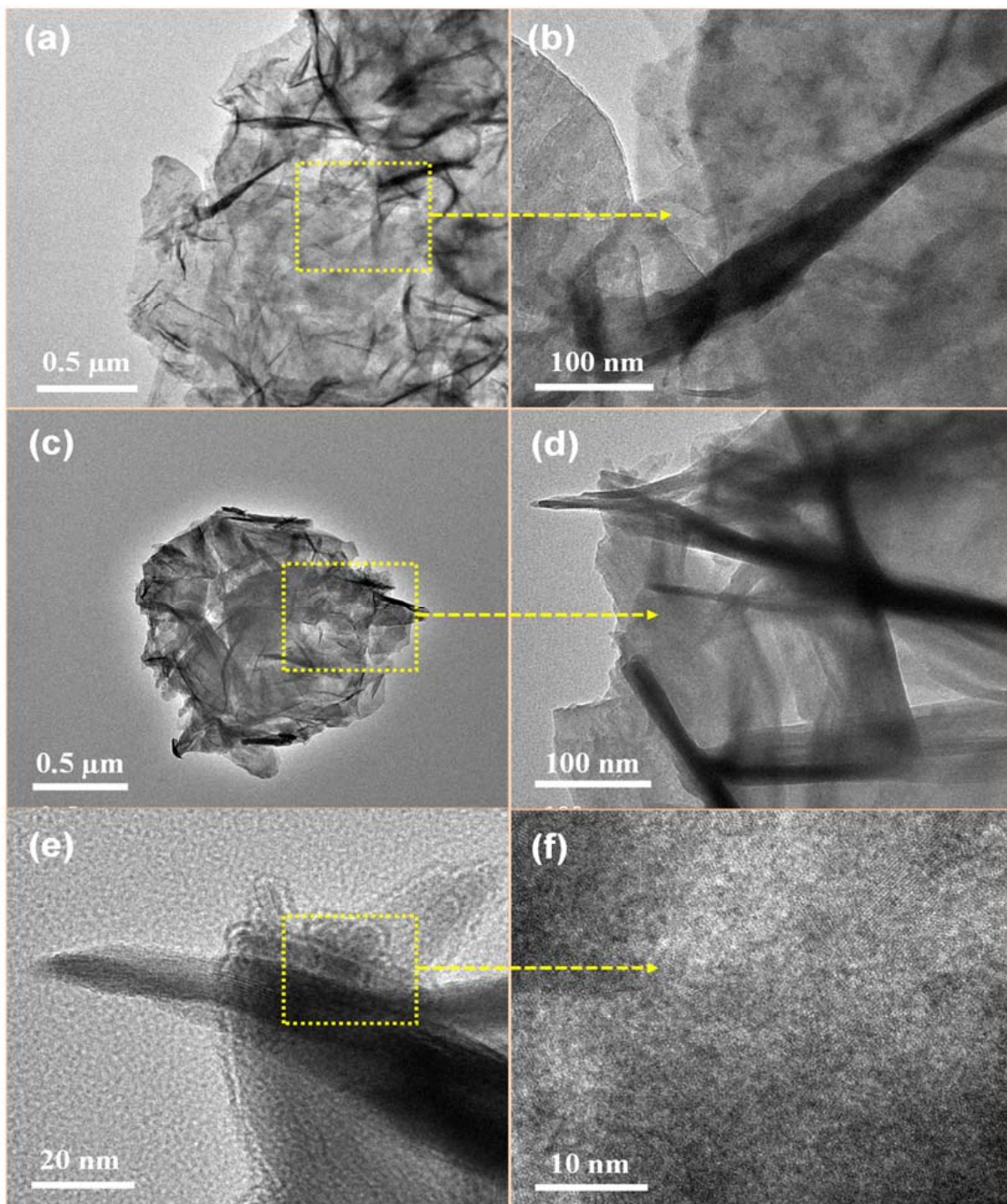


Figure 3. (a,b) TEM images of NiO, and (c–f) TEM and HRTEM images of NiZn₂O₄@3D-NF at different magnifications.

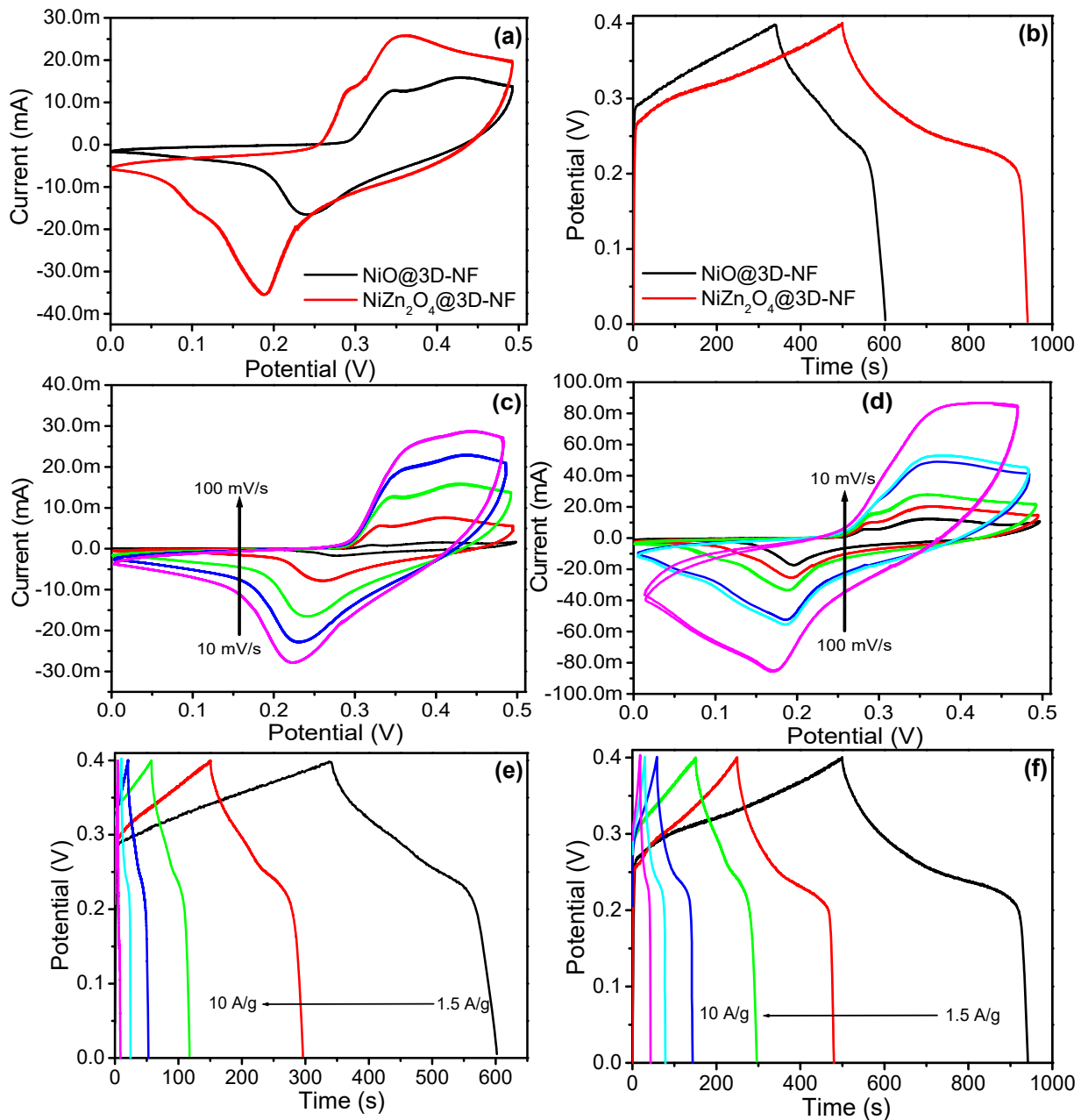


Figure 4. (a) Comparative CV of NiO@3D-NF and NiZn₂O₄@3D-NF; (b) comparative GCD graph of NiO@3D-NF and NiZn₂O₄@3D-NF; (c) CV of NiO@3D-NF at different scan rates; (d) CV of NiZn₂O₄@3D-NF at different scan rates; (e) GCD graph of NiO@3D-NF at different current densities; and (f) GCD graph of NiZn₂O₄@3D-NF at different current densities.

The supercapacitive properties were further examined using the galvanostatic charge-discharge method, which is the main technique used to evaluate the potential of electrodes in energy-storage device applications. The GCD profiles of the NiO@3D-NF and the NiZn₂O₄@3D-NF were examined at fixed and varying current densities, and the corresponding specific capacitances were calculated using the above equation (Equation (1)) [14].

The comparative GCD graph for NiO@3D-NF and NiZn₂O₄@3D-NF at fixed current densities is shown in Figure 4b, in which a clear plateau region can be observed, implying the faradaic behavior of the prepared active materials; these results are in accordance with the CV results. At a fixed current density of 1.5 A g⁻¹, the NiZn₂O₄@3D-NF delivered a specific capacitance and an areal capacitance of 1706.25 F/g (3412 mF/cm²), as well as a long discharge time, which was 1.625 times higher than that of the NiO@3D-NF (1050.0 F g⁻¹ or

2100 mF/cm²). The prolonged charge and discharge duration, the larger integrated area, and the excellent specific capacitance of NiZn₂O₄@3D-NF can be attributed to the synergy that develops because of the presence of the bimetal, which plays an important role in providing large numbers of active sites, and in facilitating increased ion diffusion during the electrochemical process. The specific capacitance of the individual electrode was also examined with the help of the GCD curves at different current densities, and the results are shown in Figure 4e,f. The resulting specific capacitance values of the NiO@3D-NF and the NiZn₂O₄@3D-NF were extracted from the GCD curves and the equation, and the results are as follows: At a current density of 1.5, 3, 4, 5, 7, and 10 A g⁻¹, the specific capacitance of the NiZn₂O₄@3D-NF was 1706.25, 1650, 1500, 1012.5, 840, and 580 F/g, respectively, and that of the NiO@3D-NF was 1050, 1012.5, 620, 400, 350, and 275 F/g, respectively (Figure 5a). These results show that the NiZn₂O₄@3D-NF delivered excellent specific capacitance performance compared to the NiO@3D-NF, as well as to other previously reported materials (Table 1).

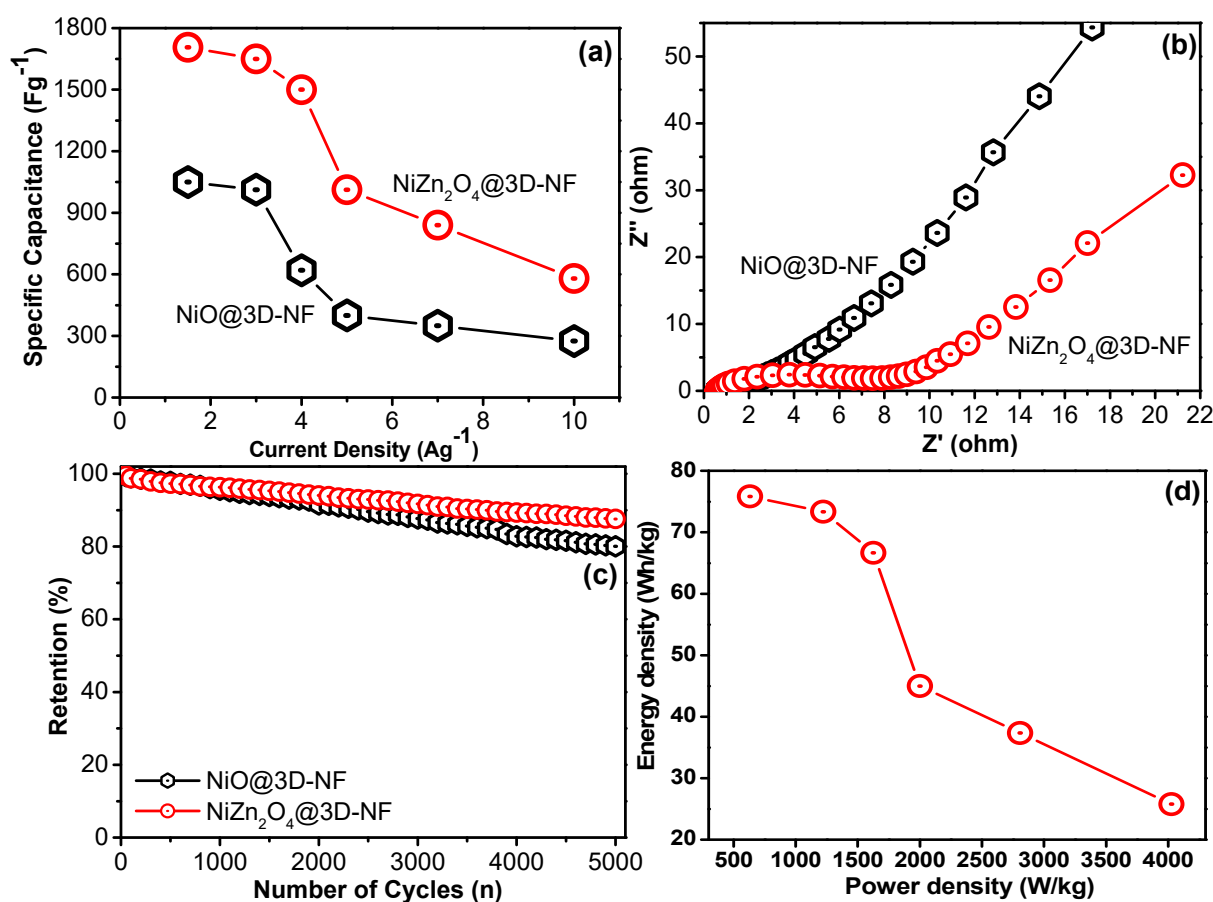


Figure 5. (a) Calculated specific capacitance of NiO@3D-NF and NiZn₂O₄@3D-NF; (b) Nyquist plot of NiO@3D-NF and NiZn₂O₄@3D-NF; (c) cycling stability graph of NiO@3D-NF and NiZn₂O₄@3D-NF; (d) Ragone plot of NiZn₂O₄@3D-NF.

The charge transfer resistance, ion diffusion, and electrical conductivity of the NiO@3D-NF and NiZn₂O₄@3D-NF electrodes were explored, and the electrochemical impedance spectroscopy technique was applied from low- to high-frequency regions, and the further results are plotted as a Nyquist plot (Figure 5b). Generally, the Nyquist plot exhibits semicircular behavior in high-frequency regions, and linear behavior in low-frequency regions [2,12,15]. The semicircle region provides information related the charge transfer resistance (R_{ct}), whereas the linear region provides information related to the Warburg impedance (W), the mass transfer, and the resistivity of the electrolyte in contact with electrodes. The Warburg impedance appears after the interaction of the OH⁻ ions with

the electrodes. Figure 5b shows that the semicircle diameter in high-frequency regions for the NiZn₂O₄@3D-NF electrodes is much smaller compared to that for the NiO@3D-NF electrodes, which indicates the fast charge transfer occurring over the NiZn₂O₄@3D-NF as compared to the NiO@3D-NF electrodes. The straight line in the low-frequency region, which makes an angle with the z-axis, clearly indicates the better energy-storage properties of the NiZn₂O₄@3D-NF over the NiO@3D-NF electrodes. Additionally, the Nyquist plot behavior also supports the pseudocapacitive behavior of the prepared electrodes [20].

Stability is a major issue of concern, and an important parameter to elucidate when investigating the potential application of energy-storage electrode materials. Thus, the consecutive charge–discharging cycle test was also conducted, and the results are shown in Figure 5c. Compared to the NiO@3D-NF, the NiZn₂O₄@3D-NF exhibited excellent cyclic stability over a 5000-cycle run at a fixed current load. The stability results also show that the specific capacitance was almost maintained over the entire long cycle, and it did not drop quickly after 1000–2000 cycles, which supports the excellent cyclic stability of the designed NiZn₂O₄@3D-NF electrode. However, compared to the NiZn₂O₄@3D-NF electrode, the specific capacitance of the NiO@3D-NF decreased much faster after 1000 charge–discharging cycles. This implies that the prepared NiZn₂O₄@3D-NF electrode has good rate capability, long-life stability, and superior specific capacitive properties, suggesting that it has great potential for energy-storage applications.

Apart from stability, the power density of the electrode is also a very important parameter, and it can be measured during the electrochemical measurements, and further calculated using Equations (2) and (3). The corresponding plots (Ragone plots) are shown in Figure 5d. From the Ragone plot, it can clearly be seen that the energy density decreased when the power density increased, which is in accordance with the calculated specific capacitance value. This behavior can be justified as follows: At a high current load, the charging process is fast, and electrolytic ions do not have sufficient time to penetrate the available pores on the electrode surface. In the present case, the constructed electrode material exhibited a maximum energy density of 75.83 Wh/kg at the power density of 631.91 W/kg. Moreover, the NiZn₂O₄@3D-NF electrode achieved the highest power density of 4026.56 W/kg, with a corresponding energy density of 25.77 Wh/kg. The maximum energy density of the NiZn₂O₄@3D-NF electrode was higher than that of several binder-free supercapacitance electrodes, such as ZCGNO/Ni foam (62.8 Wh/kg) [29], ZnCo₂O₄ nanowire array/Ni foam (41 Wh/kg) [30], and ZnCo₂O₄ nanowire cluster array/Ni foam (12.5 Wh/kg) [31].

Table 1. Overall comparison between the electrode in this study and previously reported electrodes.

No.	Electrode Material	Morphology	Synthesis Method	Synthesis Condition	Current Collector	Electrolyte	Specific Capacitance	Cyclic Stability and Retention	Ref.
1	Cobalt–nickel–zinc ternary oxide	Mesoporous nanosheet	Hydrothermal	130 °C for 5 h	Ni foam	6M KOH	1172.2 C/g (1 A/g)	81.6% @2000	[10]
2	Zinc–nickel–cobalt ternary oxide	Nanosheets	Solvothermal	120 °C for 7 h	Powder	6M KOH	257.5 F/g (0.5 A/g)	97.18% @2000	[32]
3	ZnCo ₂ O ₄ –Ni _x Co _{2x} (OH) _{6x}	Core–shell nanowire	Hydrothermal	120 °C for 5 h	Ni foam	2 M KOH	419.1 F/g (1 A/g)	81.4% @2000	[33]
4	ZnCo ₂ O ₄ /rGO/NiO	Nanowires	Hydrothermal	210 °C for 24 h	Ni foam	6 M KOH	1256 F/g (3 A/g)	80.2% @3000	[29]
5	NiZn ₂ O ₄ –NiO	Nanoleaves with nanoparticles	Hydrothermal	140 °C for 4 h	Ni foam	2 M KOH	1284.2 F/g (1 A/g)	98.17% @5000	[8]

Table 1. Cont.

No.	Electrode Material	Morphology	Synthesis Method	Synthesis Condition	Current Collector	Electrolyte	Specific Capacitance	Cyclic Stability and Retention	Ref.
6	ZnO@Ni ₃ S ₂	Core-shell nanorods	Electrodeposition	1.2–0.2 V, 5 mV/s	Ni foam	2 M KOH	1529 F/g (2 A/g)	42% @2000	[34]
7	Ni _x Zn _{1-x} S	Porous spheroid nanoparticles	Modified interface method and hydrothermal	393 K for 8 h	Powder	3 M KOH	1867 F/g (1 A/g)	77.4% @1000	[17]
8	NiO@Ni foam	Nanosheets	Hydrothermal	200 °C for 24 h	Ni foam	2 M KOH	943.5 F/g (5 A/g)	91.1% @1200	[35]
9	NiO coated NF	Nanowires	Hydrothermal	120 °C for 4 h	Ni Foam	2 M KOH	231 F/g (0.5 A/g)	-	[36]
10	NiO-NF	Nanoparticles	Sol-gel	-	Ni Foam	4 M KOH	871 F/g 5 mV/s	86.5% @10,000	[37]
11	ZnO film	Nanoparticles	Spent Zn-C battery	60 °C for 24 h	Porous silicon substrate	0.6 M KOH	547 F/g 5 mV/s	-	[38]
12	Zinc Oxide Nanorods	Pine-needle nanorod	Electrospinning	95 °C for 1 h	Nanofiber	1 M H ₂ SO ₄	56.99 F/g (0.1 mA/cm ²)	78% @5000	[39]
13	NiZn ₂ O ₄ @3D-NF	3D nanosheet assembled flower with several-burr morphology	Solvothermal	150 °C for 5 h	Ni foam	2 M KOH	1706.25 F/g (1.5 A/g)	88% @5000	Present work

As expected, all spectroscopic and microscopic analyses confirmed the identity of the prepared active materials as NiZn₂O₄@3D-NF and NiO@3D-NF electrodes. The developed binder-free electrodes also exhibited excellent electrochemical performances.

Three-dimensional active materials grown over porous nickel foam have many favorable characteristics, including corrosion resistance, high conductivity, abundant active sites for electrochemical reactions, and a high surface area, which make them suitable candidates for potential application in the field of energy storage. The synergism of the bimetallic oxides plays an important role in reducing the diffusion path length of the ions during the electrochemical reaction, which leads to the fast transportation of electrons between electrodes and electrolytes, which significantly enhances the overall capacitive performance of the electrodes (Figure 6) [40].

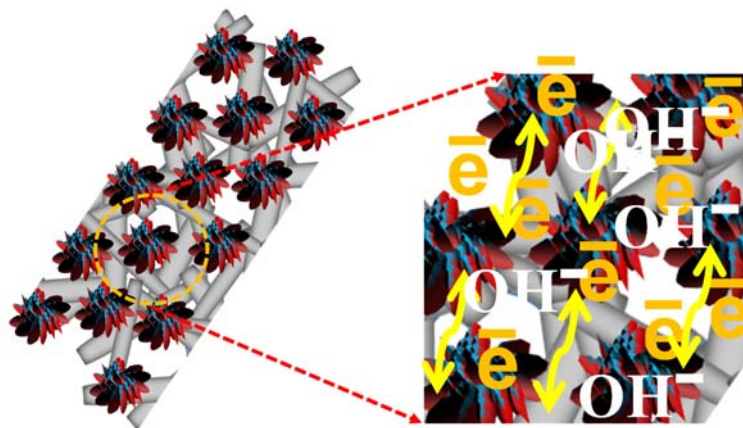


Figure 6. Expected mechanism for interaction and charge over electrodes and electrolytes during electrochemical analysis.

4. Conclusions

In this work, we prepared binder-free NiZn₂O₄@3D-NF and NiO@3D-NF electrodes through a simple and cost-effective one-step hydrothermal process. The prepared electrodes were set up in a three-electrode assembly in order to examine their electrochemical supercapacitive performance, and the results show that the developed NiZn₂O₄@3D-NF electrodes delivered a high capacitance value compared to the NiO@3D-NF electrodes. The unique three-dimensional morphology and porous behavior of the electrodes facilitate ion transport, which reduces the weight of the electrodes and provides a better liquid–solid interface, which leads to overall improved supercapacitive performance. The NiZn₂O₄@3D-NF electrode showed better cyclic stability than the NiO@3D-NF electrode at a fixed current density, which supports its durability. The prepared NiZn₂O₄@3D-NF also exhibited high power density and energy density compared to the NiO@3D-NF electrode. The excellent electrochemical supercapacitive performance demonstrates the advantages of using three-dimensional bimetallic oxide-based electrodes grown over a three-dimensional current collector, which provide better conductivity, structural stability, ion transportation, and interfacial interaction between the electrode and the electrolytes during the electrochemical reaction. The enhanced supercapacitive performance is encouraging for the potential application of NiZn₂O₄@3D-NF electrodes in various energy-storage devices.

Supplementary Materials: The following are available online at <https://www.mdpi.com/article/10.3390/cryst12010014/s1>, Figure S1: SEM image of bare nickel foam; Figure S2: CV and CD profile of the bare nickel foam.

Author Contributions: Conceptualization, methodology, writing-original draft, and project management S.A.A.; validation, methodology, investigation, review and editing N.P.; investigation and M.A.S.A.-O.; methodology, review and editing M.O.A. All authors have read and agreed to the published version of the manuscript.

Funding: This research was funded by Deanship of Scientific Research at King Faisal University for the financial support under NASHER track (Grant # 216089) and The APC was funded by Grant # 216089).

Institutional Review Board Statement: Not applicable.

Informed Consent Statement: Not applicable.

Data Availability Statement: Not applicable.

Acknowledgments: The authors acknowledge the Deanship of Scientific Research at King Faisal University for the financial support under the NASHHER track (Grant # 216089).

Conflicts of Interest: The authors declare no conflict of interest.

References

1. Javed, M.S.; Shaheen, N.; Hussain, S.; Li, J.; Shah, S.S.A.; Abbas, Y.; Ahmad, M.A.; Raza, R.; Mai, W. An ultra-high energy density flexible asymmetric supercapacitor based on hierarchical fabric decorated with 2D bimetallic oxide nanosheets and MOF-derived porous carbon polyhedral. *J. Mater. Chem. A* **2019**, *7*, 946–957. [[CrossRef](#)]
2. Parveen, N.; Ansari, S.A.; Ansari, M.Z.; Ansari, M.O. Manganese oxide as an effective electrode material for energy storage: A review. *Environ. Chem. Lett.* **2021**, 1–27. [[CrossRef](#)]
3. Ansari, S.A.; Goumri-Said, S.; Yadav, H.M.; Belarbi, M.; Aljaafari, A.; Kanoun, M.B. Directly grown of NiCo₂S₄ nanoparticles on a conducting substrate towards the high-performance counter electrode in dye-sensitized solar cell: A combined theoretical and experimental study. *Sol. Energy Mater. Sol. Cells* **2021**, *225*, 111064. [[CrossRef](#)]
4. Ansari, M.Z.; Parveen, N.; Nandi, D.K.; Ramesh, R.; Ansari, S.A.; Cheon, T.; Kim, S.H. Enhanced activity of highly conformal and layered tin sulfide (SnS_x) prepared by atomic layer deposition (ALD) on 3D metal scaffold towards high performance supercapacitor electrode. *Sci. Rep.* **2019**, *9*, 10225. [[CrossRef](#)]
5. Ashraf, M.; Shah, S.S.; Khan, I.; Aziz, M.A.; Ullah, N.; Khan, M.; Adil, S.F.; Liaqat, Z.; Usman, M.; Tremel, W.; et al. A high-performance asymmetric supercapacitor based on tungsten oxide nanoplates and highly reduced graphene oxide electrodes. *Chem.-A Eur. J.* **2021**, *27*, 6973–6984. [[CrossRef](#)]

6. Alam, M.W.; Kumar, V.G.D.; Ravikumar, C.R.; Prashantha, S.C.; Murthy, H.C.A.; Kumar, M.R.A. Chromium (III) doped polycrystalline MgAl₂O₄ nanoparticles for photocatalytic and supercapacitor applications. *J. Phys. Chem. Solids* **2022**, *161*, 110491. [[CrossRef](#)]
7. Balaji, T.E.; Das, H.T.; Maiyalagan, T. Recent trends in bimetallic oxides and their composites as electrode materials for supercapacitor applications. *ChemElectroChem* **2021**, *8*, 1723–1746. [[CrossRef](#)]
8. Kumar, Y.A.; Kumar, K.D.; Kim, H.-J. Facile preparation of a highly efficient NiZn₂O₄-NiO nanoflower composite grown on Ni foam as an advanced battery-type electrode material for high-performance electrochemical supercapacitors. *Dalton Trans.* **2020**, *49*, 3622–3629. [[CrossRef](#)]
9. Li, M.; Meng, Z.; Feng, R.; Zhu, K.; Zhao, F.; Wang, C.; Wang, J.; Wang, L.; Chu, P.K. Fabrication of Bimetallic Oxides (MCo₂O₄; M=Cu, Mn) on Ordered Microchannel Electro-Conductive Plate for High-Performance Hybrid Supercapacitors. *Sustainability* **2021**, *13*, 9896. [[CrossRef](#)]
10. Wu, C.; Chen, L.; Lou, X.; Ding, M.; Jia, C. Fabrication of cobalt-nickel-zinc ternary oxide nanosheet and applications for supercapacitor electrode. *Front. Chem.* **2018**, *6*, 597. [[CrossRef](#)] [[PubMed](#)]
11. Parveen, N.; Ansari, S.A.; Cho, M.H. Intercalated reduced graphene oxide and its content effect on the supercapacitance performance of the three dimensional flower-like β-Ni(OH)₂ architecture. *New J. Chem.* **2017**, *41*, 10467–10475. [[CrossRef](#)]
12. Ansari, S.A.; Khan, N.A.; Hasan, Z.; Shaikh, A.A.; Ferdousi, F.K.; Barai, H.R.; Lopa, N.S.; Rahman, M.M. Electrochemical synthesis of titanium nitride nanoparticles onto titanium foil for electrochemical supercapacitors with ultrafast charge/discharge. *Sustain. Energy Fuels* **2020**, *4*, 2480–2490. [[CrossRef](#)]
13. Parveen, N.; Ansari, S.A.; Ansari, S.G.; Fouad, H.; Salam, N.M.; Cho, M.H. Solid-state symmetrical supercapacitor based on hierarchical flower-like nickel sulfide with shape-controlled morphological evolution. *Electrochim. Acta* **2018**, *268*, 82–93. [[CrossRef](#)]
14. Ansari, S.A.; Parveen, N.; Kotb, H.M.; Alshoaibi, A. Hydrothermally derived three-dimensional porous hollow double-walled Mn₂O₃ nanocubes as superior electrode materials for supercapacitor applications. *Electrochim. Acta* **2020**, *355*, 136783. [[CrossRef](#)]
15. An, C.; Zhang, Y.; Guo, H.; Wang, Y. Metal oxide-based supercapacitors: Progress and perspectives. *Nanoscale Adv.* **2019**, *1*, 4644. [[CrossRef](#)]
16. Tang, X.; Zhang, B.; Lui, Y.H.; Hu, S. Ni-Mn bimetallic oxide nanosheets as high-performance electrode materials for asymmetric supercapacitors. *J. Energy Storage* **2019**, *25*, 100897. [[CrossRef](#)]
17. Wang, X.; Hu, J.; Liu, W.; Wang, G.; An, J.; Lian, J. Ni-Zn binary system hydroxide, oxide and sulfide materials: Synthesis and high supercapacitor performance. *J. Mater. Chem. A* **2015**, *3*, 23333. [[CrossRef](#)]
18. Yadav, H.M.; Ramesh, S.; Kumar, K.A.; Shinde, S.; Sandhu, S.; Sivasamy, A.; Shrestha, N.K.; Kim, H.S.; Kim, H.S.; Bathula, C. Impact of polypyrrole incorporation on nickel oxide@multi walled carbon nanotube composite for application in supercapacitors. *Polym. Test.* **2020**, *89*, 106727. [[CrossRef](#)]
19. Sahoo, S.; Nguyen, T.T.; Shim, J.-J. Mesoporous Fe-N-Co ternary oxide nanoflake arrays on Ni foam for high-performance supercapacitor applications. *J. Ind. Eng. Chem.* **2018**, *63*, 181–190. [[CrossRef](#)]
20. Zhang, J.; Liu, F.; Cheng, J.P.; Zhang, X.B. Binary nickel-cobalt oxides electrode materials for high-performance supercapacitors: Influence of its composition and porous nature. *ACS Appl. Mater. Interfaces* **2015**, *7*, 17630–17640. [[CrossRef](#)]
21. Rui, X.; Tan, H.; Yan, Q. Nanostructured metal sulfides for energy storage. *Nanoscale* **2014**, *6*, 9889. [[CrossRef](#)]
22. Liu, Y.; Li, Y.; Kang, H.; Jin, T.; Jiao, L. Design, synthesis, and energy-related applications of metal sulfides. *Mater. Horiz.* **2016**, *3*, 402. [[CrossRef](#)]
23. Wang, P.; Zhou, H.; Meng, C.; Wang, Z.; Akhtar, K.; Yuan, A. Cyanometallic framework-derived hierarchical Co₃O₄-NiO/graphene foam as high-performance binder-free electrodes for supercapacitors. *Chem. Eng. J.* **2019**, *369*, 57–63. [[CrossRef](#)]
24. Xu, X.; Gao, J.; Hong, W. Ni-based chromite spinel for high-performance supercapacitors. *RSC Adv.* **2016**, *6*, 29646–29653. [[CrossRef](#)]
25. Xu, L.; Zhao, Y.; Lian, J.; Xu, Y.; Bao, J.; Qiu, J.; Xu, L.; Xu, H.; Hua, M.; Li, H. Morphology controlled preparation of ZnCo₂O₄ nanostructures for asymmetric supercapacitor with ultrahigh energy density. *Energy* **2017**, *123*, 296–304. [[CrossRef](#)]
26. Sahoo, S.; Naik, K.K.; Rout, C.S. Electrodeposition of spinel MnCo₂O₄ nanosheets for supercapacitor applications. *Nanotechnology* **2015**, *26*, 455401. [[CrossRef](#)]
27. Xu, J.; Liu, F.; Peng, X.; Li, J.; Yang, Y.; Jin, D.; Jin, H.; Wang, X.; Hong, B. Hydrothermal synthesis of NiCo₂O₄/activated carbon composites for supercapacitor with enhanced cycle performance. *ChemistrySelect* **2017**, *2*, 5189–5195. [[CrossRef](#)]
28. Yan, D.; Wang, W.; Luo, X.; Chen, C.; Zeng, Y.; Zhu, Z. NiCo₂O₄ with oxygen vacancies as better performance electrode material for supercapacitor. *Chem. Eng. J.* **2018**, *334*, 864–872. [[CrossRef](#)]
29. Sahoo, S.; Shim, J.-J. Facile Synthesis of Three-Dimensional Ternary ZnCo₂O₄/Reduced Graphene Oxide/NiO Composite Film on Nickel Foam for Next Generation Supercapacitor Electrodes. *ACS Sustain. Chem. Eng.* **2017**, *5*, 241–251. [[CrossRef](#)]
30. Wang, S.; Pu, J.; Tong, Y.; Cheng, Y.; Gao, Y.; Wang, Z. ZnCo₂O₄ nanowire arrays grown on nickel foam for high-performance pseudocapacitors. *J. Mater. Chem. A* **2014**, *2*, 5434–5440. [[CrossRef](#)]
31. Guan, B.; Guo, D.; Hu, L.; Zhang, G.; Fu, T.; Ren, W.; Li, J.; Li, Q. Facile synthesis of ZnCo₂O₄ nanowire cluster arrays on Ni foam for high-performance asymmetric supercapacitors. *J. Mater. Chem. A* **2014**, *2*, 16116–16123. [[CrossRef](#)]
32. Shi, X.; Zhou, G. Preparation of zinc-nickel-cobalt ternary oxide nanosheets as electrodes in supercapacitors. *Chem. Res. Chin. Univ.* **2017**, *33*, 939–945. [[CrossRef](#)]

33. Fu, W.; Wang, Y.; Han, W.; Zhang, Z.; Zha, H.; Xie, E. Construction of hierarchical $\text{ZnCo}_2\text{O}_4@ \text{Ni}_x\text{Co}_{2-x}(\text{OH})_{6x}$ core/shell nanowire arrays for high-performance supercapacitors. *J. Mater. Chem. A* **2016**, *4*, 173–182. [[CrossRef](#)]
34. Xing, Z.; Chu, Q.; Ren, X.; Ge, C.; Qusti, A.H.; Asiri, A.M.; Al-Youbi, A.O.; Sun, X. Ni_3S_2 coated ZnO array for high-performance supercapacitors. *J. Power Sources* **2014**, *245*, 463–467. [[CrossRef](#)]
35. Yan, H.; Zhang, D.; Xu, J.; Lu, Y.; Liu, Y.; Qiu, K.; Zhang, Y.; Luo, Y. Solution growth of NiO nanosheets supported on Ni foam as high-performance electrodes for supercapacitors. *Nanoscale Res. Lett.* **2014**, *9*, 424. [[CrossRef](#)]
36. Kong, L.; Li, X.; Liu, M.; Ma, X.; Luo, Y.; Kang, L. A hydrothermal process for the fabrication of nickel foam based NiO and Co_3O_4 nanostructures with excellent properties for electrochemical capacitors. *Appl. Mech. Mater.* **2013**, *291–294*, 786–790. [[CrossRef](#)]
37. Dhas, S.D.; Maldar, P.S.; Patil, M.D.; Waikar, M.R.; Sonkawade, R.G.; Moholkar, A.V. Sol-gel synthesized nickel oxide nanostructures on nickel foam and nickel mesh for a targeted energy storage application. *J. Energy Storage* **2021**, 103658. [[CrossRef](#)]
38. Hassan, K.; Farzana, R.; Sahajwalla, V. In-situ fabrication of ZnO thin film electrode using spent Zn-C battery and its electrochemical performance for supercapacitance. *SN Appl. Sci.* **2019**, *1*, 302. [[CrossRef](#)]
39. Sami, S.K.; Siddiqui, S.; Shrivastava, S.; Lee, N.; Chung, C. The pine-needle-inspired structure of Zinc Oxide nanorods grown on electrospun nanofibers for high-performance flexible supercapacitors. *Small* **2017**, *13*, 1702142. [[CrossRef](#)]
40. Abdah, M.A.A.M.; Azman, N.H.N.; Kulandaivalu, S.; Sulaiman, Y. Review of the use of transition-metal-oxide and conducting polymer-based fibres for high-performance supercapacitors. *Mater. Des.* **2020**, *186*, 108199. [[CrossRef](#)]